INSTITUTE OF PHYSICS PUBLISHING PLASMA PHYSICS AND CONTROLLED FUSION

Plasma Phys. Control. Fusion **43** (2001) 559–570 www.iop.org/Journals/pp PII: S0741-3335(01)17607-4

Dynamic behaviour of the low-to-high confinement transitions in the H-1 heliac

D L Rudakov[1], **M G Shats, J H Harris and B D Blackwell**

Plasma Research Laboratory, Research School of Physical Sciences and Engineering, Australian National University, Canberra ACT 0200, Australia

Received 2 October 2000

Abstract

The dynamic behaviour of the plasma parameters, including the local electron density, electron temperature, plasma potential and their radial gradients, is studied experimentally during the transitions between low and high confinement modes (L–H transitions) in the H-1 heliac. In particular, a dynamic phenomenon occurring near the threshold conditions for the L–H transition and manifesting itself as a quasi-periodic low-frequency modulation of the local and average plasma parameters is described and discussed. A simple qualitative model for this phenomenon, referred to as L–H cycles, is suggested.

1. Introduction

Since the discovery of the H-mode in the ASDEX tokamak [1] sudden transitions to improved confinement modes have been observed in a variety of confining devices under a broad spectrum of plasma conditions (see e.g. [2] and references therein). Although the transition scenarios vary in different cases, there are a number of distinctive common features seen in all devices, allowing one to ascribe such phenomena to a single class [2].

An improved confinement mode (H-mode) has been reported in the H-1 heliac [3–6]. Although the plasma parameters in H-1 are quite different from those in most modern tokamaks and stellarators, the H-mode observed in H-1 exhibits many of the characteristic features seen in other devices. These include the steepening of the density and temperature gradients, the reduction in the density fluctuation amplitude and the increase in the radial electric field and its shear near the plasma edge after the transition to H-mode [3–6].

Spontaneous [3, 4] and induced (by changing the heating power) [5, 6] low-to-high confinement transitions (L–H transitions) in H-1 have previously been reported. In this paper we concentrate on the dynamic behaviour of such transitions. In particular, we will describe and discuss a phenomenon occurring near the threshold conditions for the L–H transition and manifesting itself as a quasi-periodic low-frequency modulation of the local and average plasma parameters.

[1] Present address: Fusion Energy Research Program, Jacobs School of Engineering, University of California, San Diego, La Jolla, CA 92093-0417, USA.

0741-3335/01/040559+12$30.00

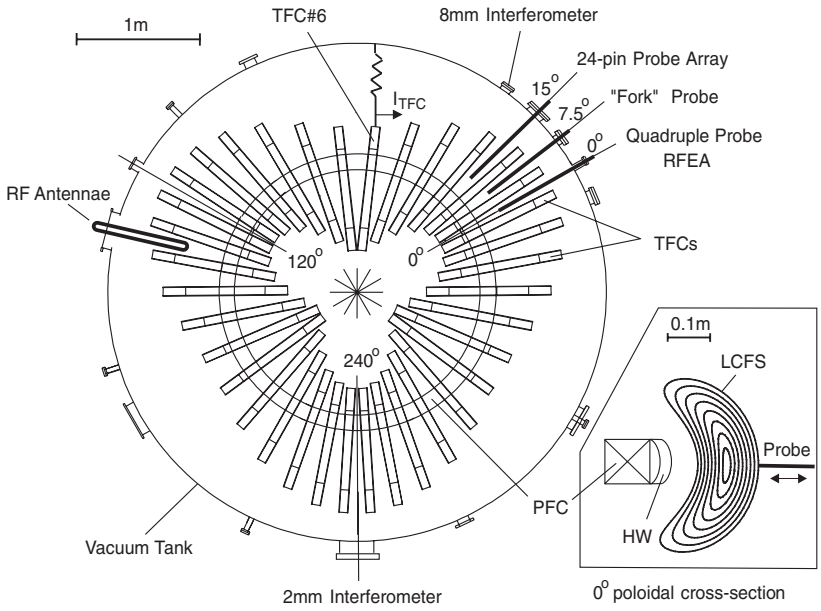

Figure 1. Experimental arrangement on the H-1 heliac.

2. Experimental arrangement

H-1 [7, 8] is a three-field-period toroidal heliac with a major radius $R = 1.0$ m and an average minor radius $\overline{a} \approx 0.15$ m. The magnetic field is created by a system of coils [7] including 36 toroidal field coils (TFCs), a poloidal field coil (PFC), two pairs of vertical field coils (VFCs) and a helical winding (HW). During the first stage of operation of H-1 (before a recent upgrade) the plasma was created and sustained by up to 100 kW of RF power at 7 MHz with a pulse duration of 30–80 ms. The experimental results presented in this paper were obtained in argon with the filling pressure $P_{\rm fill}$ of $(0.5\text{–}4)\times10^{-5}$ Torr (neutral density $n_{\rm n} \sim (0.16\text{–}1.3)\times10^{18}$ m^{-3}) and the magnetic field at the axis $B_0 = 0.04$–0.15 T in the magnetic configuration with the rotational transform $\iota \approx 1.41$ and low shear $\Delta\iota/\iota \approx 10^{-3}$ [4, 5]. The typical argon plasma parameters under such conditions are: line-averaged electron density $\overline{n}_{\rm e} \sim (0.5\text{–}1)\times10^{18}$ m^{-3}, central electron temperature $T_{\rm e}(0) \sim$ 7–20 eV, central ion temperature $T_{\rm i}(0) \sim$ 40–100 eV and average beta $\langle\beta\rangle \sim 0.2$–$0.5\%$. The plasma density profiles are peaked with the maximum gradient typically located within the region $0.5 \leqslant r/a \leqslant 0.8$ [3, 4]. The ion temperature profiles are essentially flat [4, 5]. The net toroidal current is negligible (<10 A).

The experimental arrangement on H-1 is shown in figure 1. Shown are the toroidal locations of the diagnostics, RF heating antennae, TFCs and the PFC. Inset in the right-lower corner shows a poloidal cross section of the magnetic flux surfaces at the toroidal angle $\varphi = 0^\circ$ (those at $\varphi = 120^\circ$ and $\varphi = 240^\circ$ are similar) for the configuration used in the experiments described below. Also shown are the positions of the PFC and HW. The flux surface cross sections at $\varphi = 7.5^\circ$ and $\varphi = 15^\circ$ look similar but are rotated by about 20° and 45°, respectively, around the PFC. The last-closed flux surface (LCFS) is defined as the outermost flux surface not coming in contact with internal structure elements. There are no magnetic islands or magnetic separatrices in this configuration. All probes are inserted through the areas with smoothly varying magnetic flux surface geometry.

Moderate plasma parameters in H-1 allow extensive use of different types of probe diagnostics throughout the plasma cross section [9]. The local plasma parameters, including the ion saturation current I_{si}, the electron temperature T_e and the plasma potential V_p, are typically measured with three quadruple Langmuir probes [9] (a combination of a triple probe [10] and a single probe). Two such probes are installed on a single drive (located in the $\varphi = 7.5^\circ$ cross section) allowing both radial and vertical motion. This 'fork' probe [5, 9] may thus be positioned in almost any point of the poloidal cross section. In the experiments described here the probe was moved radially along a chord passing through the plasma centre. 'Fork' probes of two different types are used. In a poloidal (symmetric) 'fork' probe the two quadruple probes are of the same length, separated by 15 mm in the poloidal direction. This arrangement allows measurements of the poloidal mode numbers of the density and potential fluctuations [6, 9]. It also allows measurements of the fluctuating poloidal electric field:

$$E_\theta = \frac{V_{p1} - V_{p2}}{d} \tag{1}$$

where V_{p1} and V_{p2} are the plasma potentials measured by the two probes and d is the poloidal probe separation. This, in turn, allows direct time-resolved measurements of the fluctuation-driven particle flux:

$$\Gamma_{fl} = \frac{1}{B_\varphi}\langle \tilde{n}\tilde{E}_\theta \rangle \tag{2}$$

where B_φ is the toroidal magnetic field.

In a radial (asymmetric) 'fork' probe [5, 9] the probe tips are separated by 15 mm in both the poloidal and the radial directions. Another radially movable quadruple probe located in the adjacent ($\varphi = 0^\circ$) poloidal cross section (see figure 1) is typically fixed at a radial position corresponding to the LCFS. This arrangement allows time-resolved measurements of both local (across 15 mm) and average (from $r/a \approx 0.3$ to $r/a \approx 1$) radial gradients of the plasma parameters measured by the probes (I_{si}, T_e and V_p). In particular, the time-resolved radial electric field E_r can be determined in a way similar to equation (1). Furthermore, since these parameters are measured simultaneously at three different radial locations, their second radial derivatives can be estimated. For example, if probes 1 and 2 are located at a radial separation of d_1 and probes 2 and 3 are located at a radial separation of d_2, the average radial electric field shear in the vicinity of probe 2 can be estimated as

$$\frac{\partial E_r}{\partial r} = -\frac{\partial^2 V_p}{\partial r^2} = -\left(\frac{V_{p3} - V_{p2}}{d_2} - \frac{V_{p2} - V_{p1}}{d_1}\right)\left(\frac{d_1 + d_2}{2}\right)^{-1} \tag{3}$$

where V_{pN} is the plasma potential measured by the Nth probe.

Time-resolved radial profiles of the ion saturation current are measured with a movable linear array of 24 single Langmuir probes distanced by 1 cm [9] (only 12 channels were used in the experiments described below). The array is located in the $\varphi = 15^\circ$ cross section. The ion temperature is measured with a four-grid retarding field energy analyser (RFEA) [4, 9]. Two microwave interferometers (2 mm and 8 mm) are used to monitor the line-averaged electron density.

The vacuum system of H-1 is based on a 'coils-in-the-tank' design [7] (see figure 1). The stainless-steel jackets of the TFCs are electrically insulated from the support structure inside the vacuum tank. They are normally grounded via tungsten filaments with a resistance of about 1 Ω. For a number of TFCs additional 1 Ω resistors were connected in series with the filaments to allow measurements of the net current to the individual coil cases (as shown in figure 1 for TFC #6). This current is typically positive (ion). The dynamic behaviour of the TFC current signals in transitional shots is generally similar to that of the ion saturation current

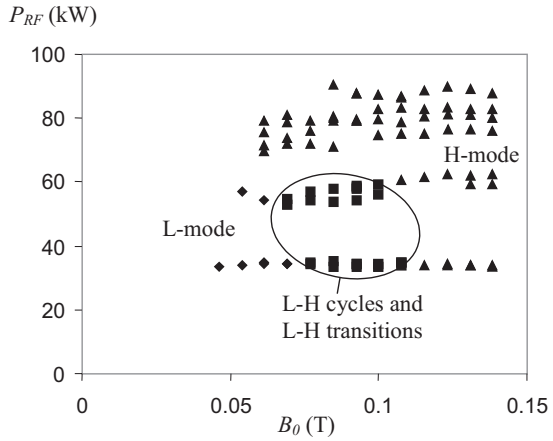

Figure 2. Operational regimes in H-1 at the filling pressure $P_{\rm fill} = 5 \times 10^{-6}$ Torr: L-mode (diamonds), L–H transitions and L–H cycles (squares), and H-mode (triangles).

to a Langmuir probe located outside the LCFS. In the experiments described below the TFC currents were used to monitor dynamic phenomena at various toroidal locations.

3. Experimental results

Figure 2 shows the typical operational domain in H-1 at a low filling pressure $P_{\rm fill}$ of 5×10^{-6} Torr (neutral density $n_{\rm n} \sim (0.16\text{–}1.3) \times 10^{18}$ m^{-3}). The data were taken in a series of discharges where the RF heating power was increased in four steps from $P_{\rm RF} \approx 35$ kW to $P_{\rm RF} \approx 90$ kW [5, 6] during the discharge, while the magnetic field was changed from shot to shot. The dependence of the operational regimes on both the RF power and the magnetic field was discussed in [5]. The L-mode and H-mode areas are clearly separated in the parameter space. In between these two areas lies the range of parameters where spontaneous (and induced by increased RF power) L–H transitions occur.

Two most typical scenarios of the L–H transitions in H-1 are illustrated in figure 3 showing the temporal evolution of the line-averaged electron density (inferred from the 8 mm interferometer signal) in two transitional shots under similar plasma conditions. A direct one-step L–H transition (figure 3(a)) occurs on a time scale of about 1–2 ms [3–6]. The transition may also proceed through an intermediate stage when the plasma parameters change in a quasi-periodic way from their typical L-mode levels towards the H-mode levels and back (as illustrated in figure 3(b)), until the transition to the H-mode finally occurs. This transition scenario is, in fact, more common than a single-step transition. We will refer to this phenomenon as L–H cycles. The typical duration of one cycle is 1–4 ms.

Figure 4(a) presents the temporal evolution of the radial profile of the ion saturation current measured with the 12-channel Langmuir probe array during the first 30 ms of a transitional shot with L–H cycles. (We note that the ion saturation current profile in H-1 is generally close to both the plasma density and the ion pressure profiles, since $I_{\rm si} \propto n_{\rm i}\sqrt{T_{\rm e} + T_{\rm i}}$ and in H-1 $T_{\rm i} > T_{\rm e}$ and $T_{\rm i}$ profiles are typically flat [4, 5].) For the purpose of clarity the signals are boxcar averaged (see the appendix, equation (A1)) over a 0.2 ms interval to remove fluctuations. It can be noticed that the density modulation in the inner region of the plasma column has an opposite phase to that at the edge. The inversion point is located at about 1 cm inside the LCFS.

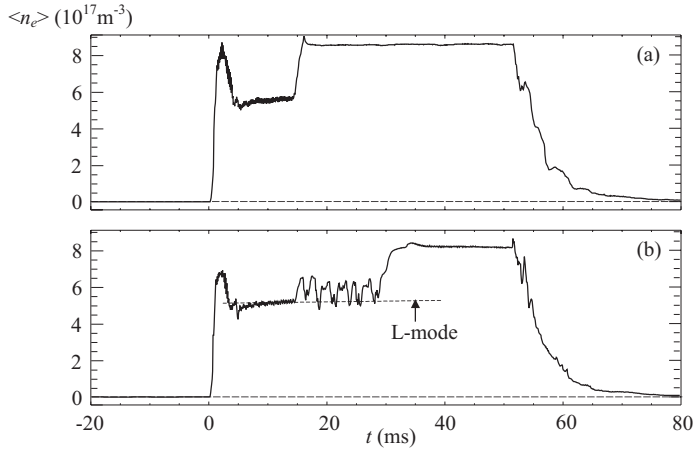

Figure 3. Temporal evolution of the line-averaged electron density during a single-step transition (a) and a transition with L–H cycles (b).

A comparison of the line-averaged signals (interferometers), poloidally-averaged signals (TFC currents) and local signals (ion saturation currents) at different toroidal and poloidal locations indicates that the modulation has toroidal and poloidal mode numbers $n = m = 0$. Therefore, it is not just a low-frequency mode, but rather a global intermittent change of the plasma conditions.

The temporal evolution of the radial profile of the density (I_{si}) fluctuation root-mean-square (RMS) amplitude (calculated as described in the appendix, equation (A2)) is shown in figure 4(b). The fluctuations observed in H-1 are highly coherent, low frequency (typically $f = 3$–12 kHz for the fundamental harmonic) and have low poloidal ($m = 1$–2) and toroidal ($n = 3$ or 6) mode numbers [6]. They exist throughout the plasma radius with the maximum level of the density fluctuations coinciding with the region of the highest pressure gradient [6] (see figure 4(b)). The fluctuations, presumably pressure-gradient-driven resistive MHD modes [6], have been shown to produce considerable turbulent particle transport [3–6].

The electron temperature, plasma potential and their corresponding fluctuation levels are also modulated in L–H cycles. Figure 5 shows the temporal evolution of the local plasma parameters measured with a quadruple probe at $r/a \approx 0.2$ in a shot with L–H cycles. Shown are the ion saturation current, figure 5(a); the plasma potential, figure 5(b); and the electron temperature, figure 5(c) (all signals are smoothed over a 0.2 ms interval). The corresponding RMS fluctuation levels (calculated as described in the appendix) are superimposed as broken curves. The fluctuation levels during L–H cycles may slightly exceed those in the L-mode and stay well above the quiescent H-mode levels.

As had been reported in [4], both toroidal and poloidal ion rotation velocities are small in H-1. Therefore, the ion pressure gradient is balanced on average by the radial electric field [4]. The modulation of the plasma density and potential in L–H cycles provides an opportunity to check if this balance is observed dynamically. As noticed above, the ion saturation current can be used as an approximate measure of the ion pressure. Figure 6(a) shows the temporal evolution of the average electric field and the average gradient of the ion saturation current (both measured between $r/a \approx 0.25$ and $r/a \approx 1$) during L–H cycles. It can be noticed that the signals are well correlated, although certain phase shifts are present.

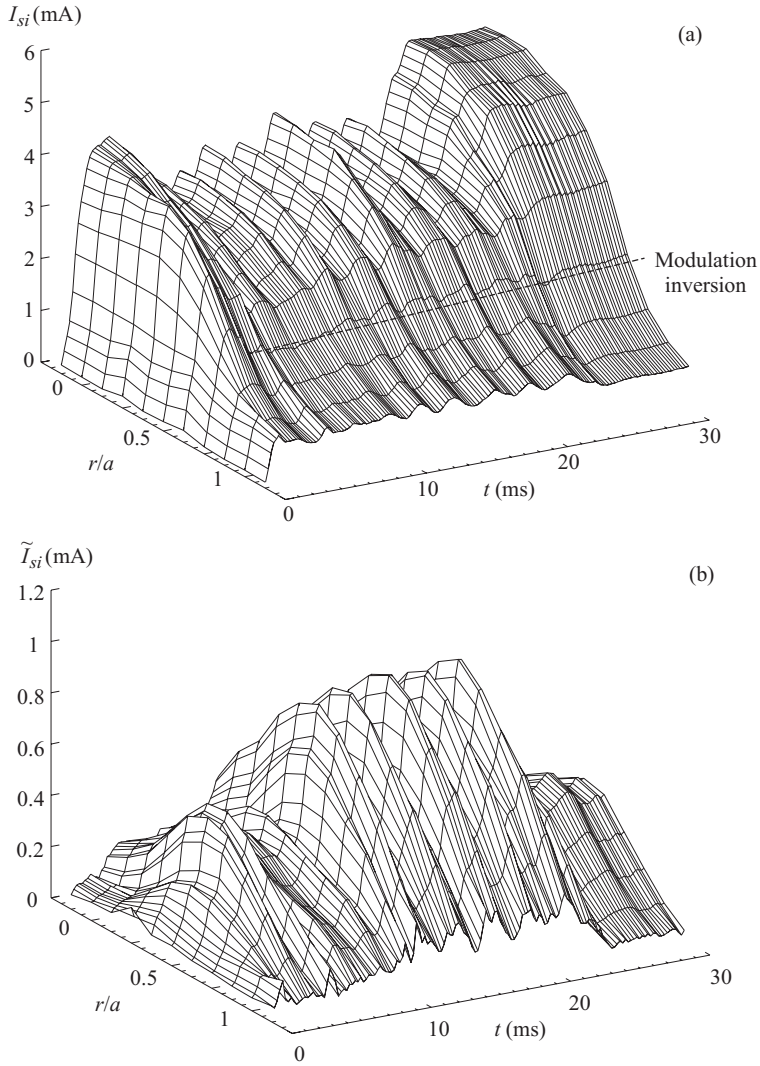

Figure 4. Temporal evolution of the radial profiles of the ion saturation current (a) and its RMS fluctuation amplitude (b) during the first 30 ms of a transitional shot with L–H cycles.

The radial electric field and its shear (radial gradient) have been shown both theoretically [11, 12] and experimentally [6, 13–16] to affect fluctuations. Here we have an opportunity to check whether this effect is important in L–H cycles. Figure 6(b) shows the temporal evolution of the ion saturation current fluctuation amplitude at $r/a \approx 0.45$ and that of the average electric field shear (determined as described in section 2, according to equation (3)) over the same time interval as the signals in figure 6(a). The correlation between the two signals is quite remarkable. In fact, all four signals in figures 6(a) and 6(b) seem correlated, which suggests their interdependence.

As mentioned above, the fluctuations in H-1 produce considerable turbulent particle flux. This flux can be measured directly using the poloidal 'fork' probe, as described in

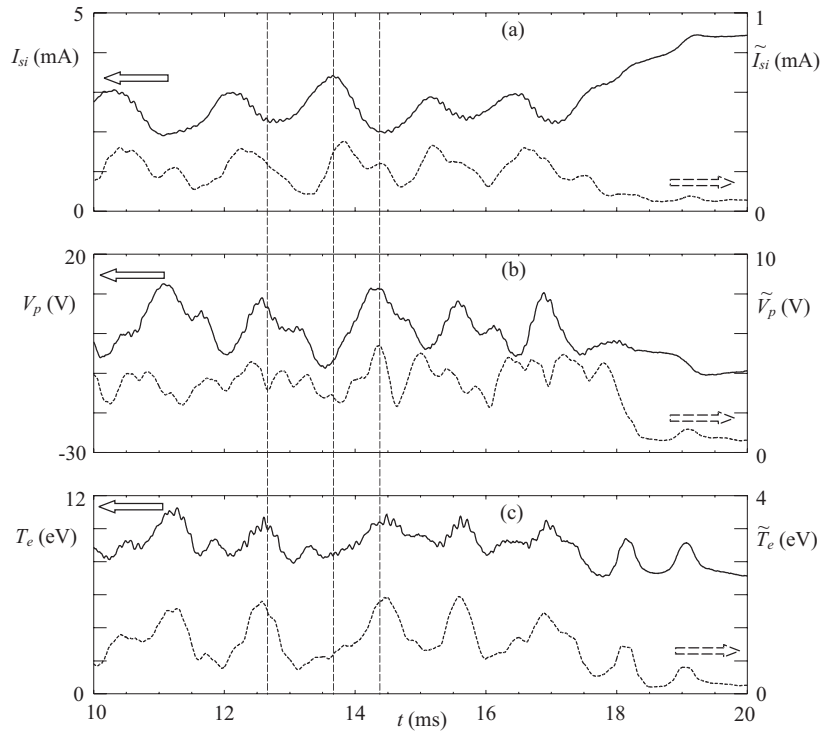

Figure 5. Temporal evolution of the ion saturation current (a), plasma potential (b), electron temperature (c) and their respective RMS fluctuation levels (broken curves) at $r/a \approx 0.2$ during L–H transition preceded by L–H cycles.

section 2. It is typically directed outwards, although it may be reversed under certain conditions [6, 17, 18]. Modulation of the fluctuation amplitudes in L–H cycles can lead to changes in the fluctuation-induced transport which, in turn, can affect the plasma density. Another factor that contributes to the changes in density is ionization. Although the average ionization rate does not change significantly across the L–H transition [4], some intermittent changes may occur. The ionization rate can be estimated as

$$I = n_{\mathrm{n}} n_{\mathrm{e}} \langle \sigma v \rangle_{\mathrm{ion}} \tag{4}$$

where n_{n} is the neutral density, n_{e} is the electron density and $\langle \sigma v \rangle_{\mathrm{ion}}$ is the ionization cross section. The latter is a strong function of the electron temperature T_{e}. The dependence is given by [19]

$$\langle \sigma v \rangle_{\mathrm{ion}} \propto \frac{1}{\sqrt{T_{\mathrm{e}}}} \exp\left(-\frac{\chi_{\mathrm{i}}}{T_{\mathrm{e}}}\right) \tag{5}$$

where χ_{i} is the ionization potential (in argon χ_{i} is 15.76 eV). Considering that $I_{\mathrm{si}} \propto n_{\mathrm{e}}\sqrt{T_{\mathrm{e}}}$, we get

$$I \propto \frac{I_{\mathrm{si}}}{T_{\mathrm{e}}} \exp\left(-\frac{\chi_{\mathrm{i}}}{T_{\mathrm{e}}}\right). \tag{6}$$

Using the latter relationship we can trace the changes in the ionization rate during L–H cycles. Figure 7(a) shows the temporal evolution of the ion saturation current I_{si} and electron

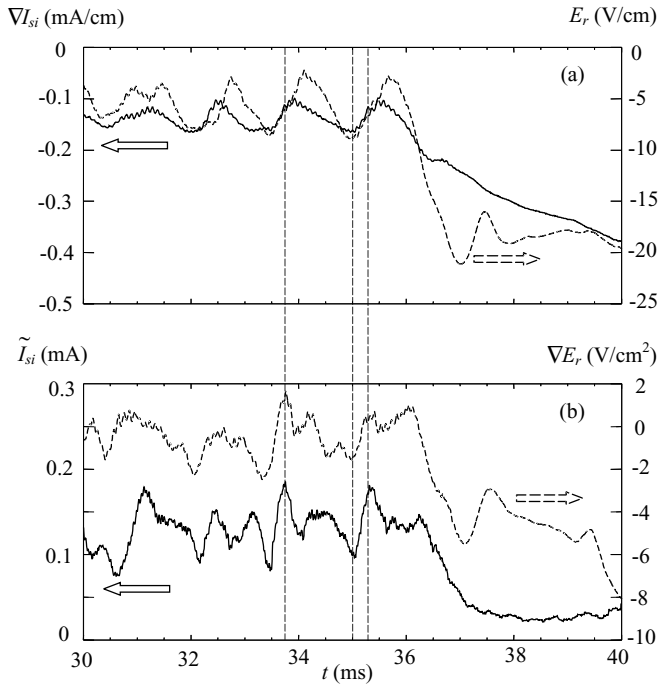

Figure 6. Temporal evolution of the average gradient of the ion saturation current (full curve, (a)), its RMS fluctuation level at $r/a \approx 0.5$ (full curve, (b)), the average electric field (broken curve, (a)) and its shear (broken curve, (b)) during L–H cycles.

temperature T_e at $r/a \approx 0.5$. It can be noticed that the temperature has a lower relative modulation than I_{si} (and hence n_e). Shown in figure 7(b) are two traces, one of which (upper) is proportional to the local ionization rate (equation (6)) and the other (lower) is proportional to the fluctuation-driven particle flux (see equation (2)). Both signals are in arbitrary units, with their common zero level shown by a broken line. Positive values of the particle flux correspond to the outward direction. Modulation of the ionization rate in L–H cycles appears to be comparatively weak and has a phase close to that of the density (I_{si}) modulation. In contrast, fluctuation-driven particle flux changes considerably, even slightly reversing at times. There is an increase in the ionization rate just before the final L–H transition, after which it returns to about the original level. The fluctuation-induced particle flux stays low after the transition.

4. Discussion and summary

L–H cycles in H-1 result in the modulation of most of the plasma parameters and periodical changes in many processes. Such changes may be interdependent in a number of ways. In particular, ionization, average density, density gradient, electric field and its shear fluctuations and fluctuation-induced particle transport may form an interdependent loop of events responsible for the appearance of L–H cycles. This loop is broken when the L–H transition finally takes place. Here we will discuss one of possible scenarios that may result in the appearance of cycles like those observed. This scenario will be substantiated by the results presented in the previous section.

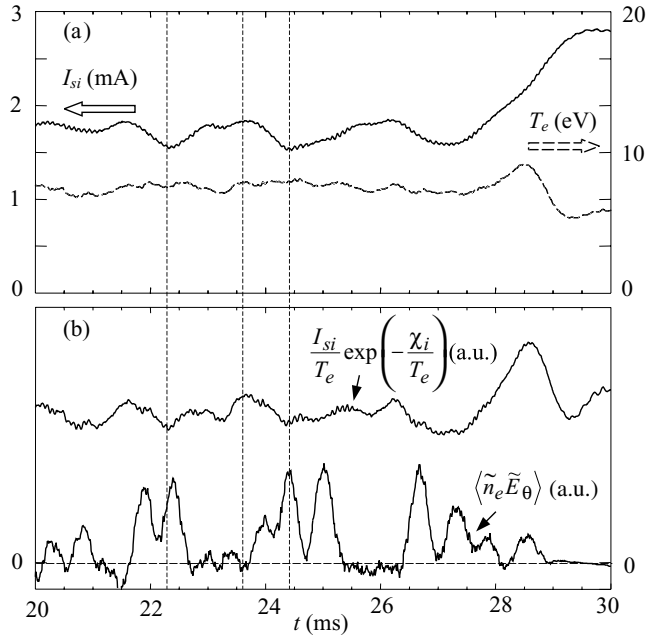

Figure 7. Temporal evolution of the ion saturation current (full curve, (a)), electron temperature (broken curve, (a)), a signal proportional to the local ionization rate (upper trace, (b)), and a signal proportional to the fluctuation-driven particle flux (lower trace, (b)) at $r/a \approx 0.5$ during L–H cycles. Positive values of the particle flux correspond to the outward direction.

A possible scenario is shown schematically in figure 8. Let us explain the diagram in figure 8 starting with the outer circle (full arrows). An increase in the central density n_0 results in an increase in the average density gradient (provided the edge density does not increase, as in figure 4(a)). If the temperature does not decrease significantly (which is generally the case), the pressure gradient also increases. The latter is presumably the driving force for the fluctuations [6], so an increased pressure gradient results in an increase in the fluctuation amplitude (see figures 5(a), 6(a) and (b)). This causes an increase of the fluctuation-driven particle flux, which eventually decreases the central density. The density and pressure gradients are consequently reduced, fluctuation levels and transport decrease, and the system eventually returns to the initial state. In fact, the large circle in figure 8 involves a negative feedback loop for the density changes: an increase in n_0 eventually stabilizes itself through enhanced particle transport. If this feedback was fast enough, no cycles would take place. However, it takes time for the local plasma parameters to change and for the profiles to be modified. Time (phase) delays in modulation of different plasma parameters are clearly visible in figures 4–7. Those delays may cause the system to oscillate.

The simple pattern discussed above involves periodical changes in the plasma parameters consistent with the experimental results (figures 4–7). However, it does not include the effect of the radial electric field and its shear on the fluctuations. As illustrated in the previous section, this effect is potentially important (see figure 6(b)) and should not be ignored. It is included in the diagram in figure 8 inside the main circle (broken arrows). An increase in the pressure gradient leads (through the radial force balance) to an increase in E_r (see figure 6(a)). Consequently, the electric field shear may increase as well. Figure 6 shows that it is usually the case, although the changes in E_r and ∇E_r are not perfectly correlated. Both E_r

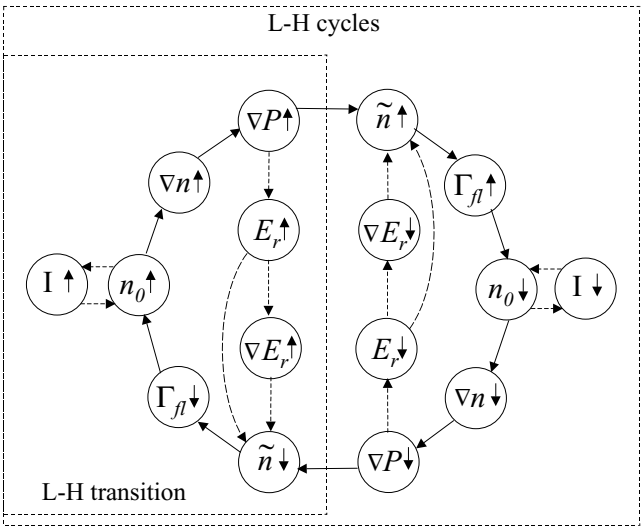

Figure 8. Suggested sequence of events during L–H cycles and L–H transition. Here n_0 denotes the central plasma density, $\tilde{n}$ is the density fluctuation amplitude, P is the total plasma pressure ($P = P_e + P_i = n(T_e + T_i)$), I denotes ionization, Γ_{fl} is the fluctuation-induced particle flux, E_r is the radial electric field and ∇E_r is the radial electric field shear. An arrow pointing up denotes an increase in the absolute value of the corresponding parameter (E_r and all radial gradients actually become more negative), an arrow pointing down denotes a decrease.

and ∇E_r may affect the fluctuations. An increase in E_r and/or ∇E_r results in a decrease in the fluctuation amplitude, which in turn decreases the particle transport and tends to further increase the central density. Similarly, a decrease of n_0 would lead (through a decrease in the density and pressure gradients) to a decrease in E_r and ∇E_r, leading to an increase in the fluctuation amplitude and transport, and would thus cause a further decrease of n_0 (right-hand side of figure 8). Therefore, the radial electric field provides a positive feedback for the density changes. The same consideration applies to ionization. Since the ionization rate in L–H cycles changes approximately in phase with the density (figure 7(b)), it would also tend to amplify any increase or decrease of the latter (small side loops in figure 8).

The effects of ionization and radial electric field may affect the L–H cycles in different ways. They may increase the modulation amplitude by providing a positive feedback, or affect the period (for example, by changing the transport rates). In fact, such effects may trigger the onset of the L–H cycles in the first place. On the other hand, they are even more likely to be responsible for the final transition to the H-mode. It has been found in H-1 that the radial electric field before the transition must always reach some critical (negative) value [5, 6]. It has also been reported [6] that the radial electric shear becomes more negative after the transition to a 'quiescent' H-mode (i.e. an H-mode where the fluctuations are suppressed [3–6]). This is also well illustrated in figure 6(b). The suppression of the fluctuations by E_r shear is generally consistent with experimental data in H-1 [6] (and with the data in figure 6 in particular). Therefore, the L–H transition to the 'quiescent' H-mode may follow the left-hand side of the diagram in figure 8. If for some reason the increase of the density is not slowed fast enough by the increased transport, the radial electric field and its shear may reach critical values, after which the fluctuations are fully suppressed and the sequence of events causing L–H cycles is broken. An ionization surge like that occurring just before the transition in figure 7(b) may contribute to the fast density increase. The L–H transition thus follows the left-hand side of the diagram in figure 8.

The pattern suggested above is consistent with experimental results for both L–H cycles and a transition to the 'quiescent' H-mode. It may also work for a transition to a 'fluctuating' H-mode [6, 17, 18], although in the latter case it would require a different modification of the E_r profile, leading to recorrelation of fluctuations rather than their suppression. (The recorrelation of the density and potential fluctuations to a different relative phase results in a change in the turbulent transport [17, 18].) In any case, the aim of the above discussion was to suggest a simple qualitative model for L–H cycles based on the experimental results. A quantitative model would be very desirable, but the development of such a model is beyond the scope of this paper.

Finally, we notice that the L–H cycles observed in H-1 to an extent resemble the so-called dithering cycles observed in tokamaks [20–22] and stellarators [23, 24] operating in the H-mode. Dithering cycles can be viewed as a series of repetitive L–H–L transitions [22]. Just like dithering cycles in other machines, L–H cycles in H-1 are observed close to the threshold conditions for the L–H transition, and improvement in confinement during the cycles is not significant compared to the L-mode. As in dithering cycles, the 'low' phase of the L–H cycles is close to the L-mode (see figure 3). During the 'high' phase of the L–H cycles most of the plasma parameters approach their H-mode values (figures 5–7). However, the fluctuations are never fully suppressed and H-mode conditions are never reached. Therefore, L–H cycles in H-1 may be viewed as a series of incomplete transitions.

Another difference between the L–H cycles in H-1 and dithering cycles is that the plasma parameters in H-1 are modulated throughout the plasma cross section, whereas in larger devices the modulation is often limited to the plasma periphery. This may be due to the global nature of the fluctuations in H-1 [3–6] (see also figure 4(b)). The reduction of the fluctuation levels in H-1 results in a decrease in the fluctuation-driven particle transport throughout the plasma cross section, which affects the central plasma density to a larger extent than in tokamaks, where the fluctuations are mainly suppressed in a narrow region close to the plasma edge.

The physical picture of the dithering cycles is generally accepted to be that of a limit cycle oscillation associated with a hysteresis in the L–H transition [22]. It is difficult to say whether the L–H cycles also show hysteresis. At first glance, the experimental data presented in figures 5–7 do not exhibit any bifurcation or hysteresis-like behaviour during the L–H cycles. However, there is not enough evidence to exclude this possibility either. A quantitative model, analytical or numerical, may reveal some kind of a limit cycle. The simple qualitative scheme in figure 8 based on experimental evidence may provide initial input for such a model while the data presented in this paper may be used for benchmarking. However, the development of a quantitative model for L–H cycles (and L–H transitions) in H-1 is still a matter for the future.

Acknowledgments

The authors would like to thank the H-1 operating team (J Wach, R Davies, R J Kimlin, G McCluskey and C Costa) for their support during the experiments.

Appendix

When dealing with dynamic phenomena involving changing fluctuation levels it is sometimes convenient to separately trace the temporal evolution of the mean value of a signal and its fluctuation amplitude. The well known 'boxcar average' procedure provides a simple way to monitor the time-resolved mean value of a signal. The boxcar average of a width w produces an output array Y in which every ith element Y_i (except for the first and the last $w/2$ elements)

is equal to the average of w elements (from $i - w/2$ to $i + w/2$) of the input array X:

$$Y_i = \frac{1}{w}\sum_{j=0}^{w-1} X_{i+j-w/2}. \tag{A1}$$

This procedure is equivalent to low-pass filtering where the bandwidth is defined by the width w (and, of course, the sampling interval). The advantage of boxcar averaging is that it does not shift the phase of the lower frequency perturbations in the signal.

The procedure used to calculate the time-resolved fluctuation levels used in this paper is based on the same principle as boxcar averaging. It produces an output array Y in which every ith element Y_i (except for the first and the last $w/2$ elements) is equal to the RMS deviation of w elements (from $i - w/2$ to $i + w/2$) of the input array X from their mean value:

$$Y_i = \left[\frac{1}{w}\sum_{j=0}^{w-1}\left(X_{i+j-w/2} - \frac{1}{w}\sum_{j=0}^{w-1} X_{i+j-w/2}\right)^2\right]^{1/2}. \tag{A2}$$

This simple yet effective procedure is equivalent to high-pass filtering with subsequent amplitude detection. It allows one to monitor changes of the fluctuation amplitudes occurring on time scales longer that $w\Delta t$, where Δt is the sampling interval.

References

[1] Wagner F *et al* 1982 *Phys. Rev. Lett.* **49** 1408
[2] Burrell K H 1994 *Plasma Phys. Control. Fusion* **36** A291
[3] Shats M G, Rudakov D L, Blackwell B D, Borg G G, Dewar R L, Hamberger S M, Howard J and Sharp L E 1996 *Phys. Rev. Lett.* **77** 4190
[4] Shats M G, Rudakov D L, Boswell R W and Borg G G 1997 *Phys. Plasmas* **4** 3629
[5] Shats M G, Michael C A, Rudakov D L and Blackwell B D 1998 *Phys. Plasmas* **5** 2390
[6] Shats M G 1999 *Plasma Phys. Control. Fusion* **41** 1357
[7] Hamberger S M, Blackwell B D, Sharp L E and Shenton D B 1990 *Fusion Technol.* **17** 123
[8] Shats M G, Rudakov D L, Blackwell B D, Sharp L E, Tumlos R, Hamberger S M and Fedyanin O I 1994 *Nucl. Fusion* **34** 1653
[9] Rudakov D L, Shats M G, Boswell R W, Charles C and Howard J 1999 *Rev. Sci. Instrum.* **70** 476
[10] Chen S-L and Sekiguchi T 1965 *J. Appl. Phys.* **36** 2363
[11] Biglari H, Diamond P H and Terry P W 1990 *Phys. Fluids* B **2** 1
[12] Shaing K C, Crume E C Jr and Houlberg W A 1990 *Phys. Fluids* B **2** 1492
[13] Doyle E J, Groebner R J, Burrell K H, Gohil P, Lehecka T, Luhmann N C Jr, Matsumoto H, Osborne T H, Peebles W A and Philipona R 1991 1990 *Phys. Fluids* B **3** 2300
[14] Moyer R A, Burrell K H, Carlstrom T N, Coda S, Conn R W, Doyle E J, Gohil P, Groebner R J, Kim J and Lehrner R 1995 *Phys. Plasmas* **2** 2397
[15] Burrell K H 1999 *Phys. Plasmas* **6** 4418
[16] Boedo J A, Terry P W, Gray D, Ivanov R S, Conn R W, Jachmich S and van Oost G 2000 *Phys. Rev. Lett.* **84** 2630
[17] Shats M G and Rudakov D L 1997 *Phys. Rev. Lett.* **79** 2690
[18] Shats M G, Toi K, Ohkuni K, Yoshimura Y, Osakabe M, Matsunaga G, Isobe M, Nishimura S, Okamura S and Matsuoka K 2000 *Phys. Rev. Lett.* **84** 6042
[19] Kato T, Masai K and Arnaud M 1991 *NIFS Research Report* NIFS-DATA-14, ISSN 0915-6364, Nagoya, Japan
[20] Zohm H 1994 *Phys. Rev. Lett.* **72** 222
[21] Zohm H, Ryter F, Fuchs C, Herrmann A, Kaufmann M, Neuhauser J and Salmon N 1994 *Plasma Phys. Control. Fusion* **36** A129
[22] Zohm H 1996 *Plasma Phys. Control. Fusion* **38** 105
[23] Hirsch M *et al* 1998 *Plasma Phys. Control. Fusion* **40** 631
[24] Hirsch M *et al* 2000 *Plasma Phys. Control. Fusion* **42** A231